Effect of the third resonance on the angular distributions for electron-pyrimidine scattering

Eur. Phys. J. D (2016) 70: 151
DOI: 10.1140/epjd/e2016-70165-x

THE EUROPEAN PHYSICAL JOURNAL D

Regular Article

Effect of the third π^* resonance on the angular distributions for electron-pyrimidine scattering*

Zdeněk Mašín[1,a] and Jimena D. Gorfinkiel[2,b]

[1] Max-Born Institute for Nonlinear Optics and Short Pulse Spectroscopy, Max-Born-Strasse 2A, 12489 Berlin, Germany
[2] Department of Physical Sciences, The Open University, Walton Hall, Milton Keynes, MK7 6AA, UK

Received 4 March 2016 / Received in final form 19 May 2016
Published online 12 July 2016

Abstract. We present a detailed analysis of the effect of the well known third π^* resonance on the angular behaviour of the elastic cross section in electron scattering from pyrimidine. This resonance, occurring approximately at 4.7 eV, is of mixed shape and core-excited character. Experimental and theoretical results show the presence of a peak/dip behaviour in this energy range, that is absent for other resonances. Our investigations show that the cause of the peak/dip is an interference of background p-wave to p-wave scattering amplitudes with the amplitudes for resonant scattering. The equivalent resonance in pyrazine shows the same behaviour and the effect is therefore likely to appear in other benzene-like molecules.

1 Introduction

Electron [1–5] and positron (see [6] and references therein) scattering from pyrimidine have received significant amounts of attention in the last few years, with a number of experiments and calculations [7–10] carried out. The main reason for this interests is that pyrimidine serves as a model for the pyrimidinic nucleobases thymine, cytosine and uracil. Since experimental work [11] confirmed that low energy electrons can damage DNA via dissociative electron attachment (DEA), there has been significant interest in understanding electron scattering from DNA components [12] and in particular the formation and characteristics of the resonances that lead to DEA. From the computational point of view, the higher symmetry of pyrimidine reduces the size of the calculation and therefore allows for more sophisticated and detailed calculations than for the nucleobases. This, in turn, allows for a better comparison with experiment.

A detailed study of low energy electron scattering from pyrimidine and its isomers using the R-matrix method [9] revealed the presence of a large number of resonances. Three of these, of π^* character, were first identified by Nenner and Schulz [13] and confirmed later by experiments [2] and calculations [1,9]: the lowest two are pure shape resonances but the third one is of mixed shape core-excited character [7,9,13]. The effect these resonances have on the angular behaviour of the elastic cross section has not been investigated in detail.

Recent experiments [14,15] have provided a very detailed analysis of both elastic and inelastic (mainly electronic excitation) electron scattering from pyrimidine: the determination of both differential and integral cross sections as well as excitation functions has enabled a thorough comparison with theory. An interesting feature in the excitation functions (angular differential cross sections plotted for a specific scattering angle as a function of scattering energy) is the presence of a peak/dip in the energy range of the third π^* resonance [14]. This feature is particularly visible for backward scattering angles. This behaviour is confirmed by calculations using the R-matrix and Schwinger multichannel methods that also show the feature as a dip/peak for angles below 45°. Although no indication of these dip/peaks has been reported in other systems, this may be due to the large energy spacing used. The other π^* resonances in pyrimidine do not lead to the observation of this behaviour in the computed excitation function (the resonances are too narrow to be observed in the experiments), nor is it apparent for the core-excited shape resonances that appear above 5 eV. We present here an investigation, using the R-matrix method, of the origin of the peak/dip behaviour linked to the third π^* resonance. Section 2 introduces very briefly the methodology used while Section 3 summarizes the details of the calculation. Sections 4 and 5 present our results and conclusions respectively.

* Contribution to the Topical Issue "Advances in Positron and Electron Scattering", edited by Paulo Limao-Vieira, Gustavo Garcia, E. Krishnakumar, James Sullivan, Hajime Tanuma and Zoran Petrovic.

[a] e-mail: masin@mbi-berlin.de
[b] e-mail: J.Gorfinkiel@open.ac.uk

2 The R-matrix method and computation of the differential cross sections

The R-matrix method and its application to electron-molecule collisions is well established. We provide a brief summary below and refer the reader to earlier publications [16,17] for a detailed description. We apply the method within the fixed-nuclei approximation. For the calculations presented here we have used the UKRmol+ suite, a re-engineered version of the UKRmol codes [18]. The use of the new suite enabled us to perform calculations in quadruple precision and thus improve the quality of the continuum description (by retaining all continuum functions in the diagonalization step [18]).

The R-matrix method is based on the division of space by a sphere of radius a. This sphere defines: (i) an inner region where the scattering electron is indistinguishable from the target electrons and correlation and exchange effects play an important role; (ii) an outer region where exchange between the scattering electron and electrons of the target molecule can be neglected. The radius a must be chosen so that the charge densities of the relevant electronic target states and orbitals are fully contained inside the R-matrix sphere.

In the inner region, a set of basis functions Ψ_k describe the system. These are determined by diagonalising the non-relativistic hermitian Hamiltonian (hermiticity is ensured by addition of the Bloch operator [16]) of the $N+1$ electron system. Whether a single or several target states are included in the expansion of the Ψ_k determines whether the calculations use the Static-Exchange/Static-Exchange plus Polarization or Close-Coupling approximation.

Having obtained the basis functions Ψ_k, the R-matrix is constructed at the boundary between regions and propagated through the outer region to an asymptotic distance, where the K-matrix is determined by matching to known asymptotic expressions. In the outer region, the interaction potential between the scattering electron and those of the target is approximated with a single-centre expansion [17]. In our calculations, we restrict ourselves to including the dipolar and quadrupolar interactions.

Once the K-matrices are obtained, it is trivial to determine the T-matrices using:

$$\mathbf{T} = 2\imath\mathbf{K}(1-\imath\mathbf{K})^{-1}. \quad (1)$$

In the following we will refer to the integral elastic cross sections which, for electron incoming with momentum k, are calculated using the equation:

$$\sigma(E) = \frac{\pi}{k^2}\sum_{\Gamma}\sum_{S}\sum_{l,l'}\sum_{m,m'}\frac{2S+1}{2}|T^{\Gamma}_{l,m;l',m'}(E)|^2, \quad (2)$$

where S is the total spin of the system, Γ runs over all irreducible representations of the molecular point group and l and m define the angular behaviour of the scattering electron.

The differential cross sections (DCS) have the form

$$\frac{d\sigma}{d\Omega} = \sum_{L} A_L P_L(\cos\theta), \quad (3)$$

where $P_L(\cos\theta)$ are the Legendre polynomials and θ is the scattering angle measured with respect to the incident electron beam. The coefficients A_L are determined from the molecular-frame T-matrix elements using an adapted version of POLYDCS [19]. The full expression for the A_L coefficients is complicated but for our purposes it is only important to remember that the A_L coefficients are ultimately a function of the sum of products of the type $T_{l_1,m_1;l_1',m_1'}T^{*}_{l_2,m_2;l_2',m_2'}$ with the summation running over all combinations of the l, m indices.

POLYDCS generates rotationally resolved DCS. This reintroduces their dependence on the initial and final rotational states of the target molecule. Our elastic differential cross sections are calculated summing over final rotational states (and assuming the molecule is initially in the ground rotational state). Convergence with the number of final rotational states must be checked.

3 Characteristics of the calculation

The R-matrix results presented here were determined using the cc-pVDZ basis set and CASSCF orbitals obtained from a (10,8) active space (i.e. 10 electrons are distributed over 8 active orbitals) using MOLPRO [20]. These were used to generate the electronic wavefunctions of the ground and 28 excited states that were then included in the Close-Coupling scattering calculation. The R-matrix radius a was set to 13 a_0 and continuum functions with $l \leq 5$ were employed. Further details of the calculations can be found in earlier work [8,9]. We note here that polarization effects are usually underestimated by our Close-Coupling calculations for diazines and similar molecules [9]. For this reason shape resonances tend to appear at higher energy in our calculations than in the experiment.

Pyrimidine is a dipolar molecule belonging to the C_{2v} point group. This means that the sum over L in equation (3) is unconstrained and diverges in the fixed-nuclei approximation. This problem is normally remedied using a Born correction for a rotating dipole. However, no Born correction is included in the calculations shown below which focus on the analysis of the DCS arising from a structure due to low angular momenta. Pyrimidine is an asymmetric top, but two of its rotational constants differ by about 5%. This allows us to approximate it by a symmetric top. The calculations included final rotational states up to $j = 9$ and the DCS were obtained combining T-matrices for all doublet scattering symmetries.

The first π^* resonance in pyrimidine appears in the $^2A_2$ symmetry (around 0.5 eV in our calculations) and the other two in the $^2B_1$ symmetry (around 0.7 eV and 4.7 eV respectively). The resonance of interest is the second one of $^2B_1$ symmetry and it forms in a number of partial wave scattering channels. The elastic scattering channels for this symmetry are listed in Table 1.

Table 1. All partial wave channels (corresponding to real spherical harmonics) of the continuum electron contributing to scattering in $^2B_1$ symmetry from the ground electronic state of pyrimidine included in our calculation.

i (channel index)	l	m
1	1	1
2	2	1
3	3	1
4	3	3
5	4	1
6	4	3
7	5	1
8	5	3
9	5	5

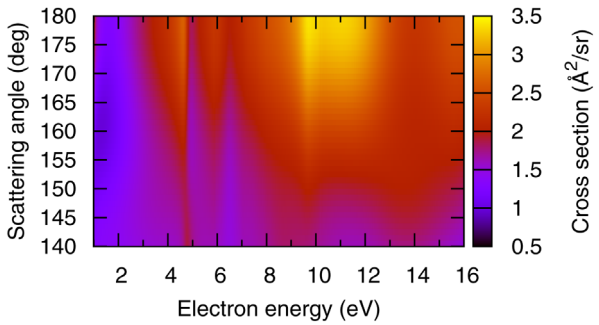

Fig. 1. Angular distributions for elastic scattering from pyrimidine for large scattering angles as a function of scattering energy.

4 Results

Figure 1 shows the calculated electron angular distribution for pyrimidine for scattering angles above 140° as a function of the scattering energy. The sharp cut-off in the angular distribution just above the energy of the 3rd π^* resonance (4.7 eV in these calculations) is clearly visible. Figure 1 also shows an enhancement of the scattering cross section in the energy range 7–13 eV which is caused by a pair of overlapping resonances (identified as $\tilde{g}\ ^2B_1$ and $\tilde{x}\ ^2B_1$ in Ref. [15]). This higher energy enhancement is smooth and does not show a cut-off effect (nor does the experimental excitation function for 180°). As stated above, this cut-off behaviour is not visible either in the energy range of the first two π^* resonances which are not shown in the figure.

The cut-off is linked to the structure which manifests itself in the calculated excitation functions as a dip/peak in the forward direction, a peak/dip structure in the backward direction and a simple peak at 90° (see Fig. 2). This cut-off is also nicely visible in the experimental excitation functions for 180° [14] where it appears as a peak/dip structure. (The variation in the forward direction for 25° is a bit harder to see in the experiment [14] since it is superimposed on the strong forward-peaking dipolar background. On the other hand, the peak at 90° which separates the forward and backward scattering is nicely visible). The forward and backward scattering behaviour

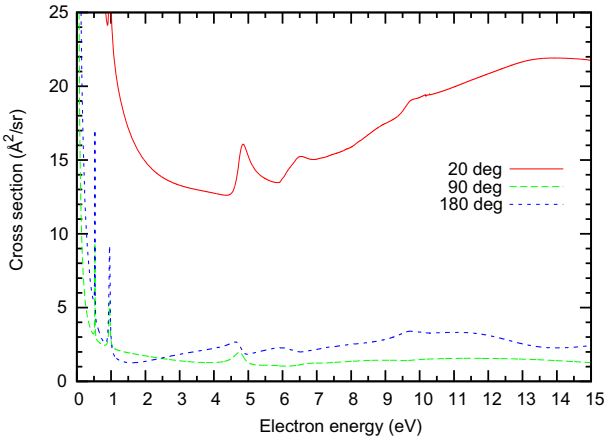

Fig. 2. Excitation functions for 20° (red line), 90° (green line) and 180° (blue line).

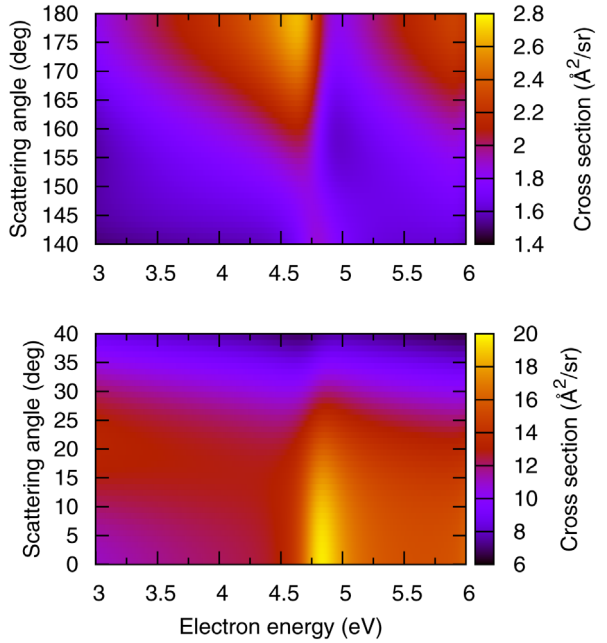

Fig. 3. Detail of the angular distributions in the energy range of the third π^* resonance for forward (lower panel) and backward (upper panel) scattering. Note the colour scales are different for each panel.

in the vicinity of the resonance is clearly illustrated in Figure 3.

The most useful clue to what is happening is provided by the contributions of the individual T-matrix elements T_{ij} (where i and j denote the channels listed in Tab. 1) to the integral elastic cross section for the $^2B_1$ symmetry. These are shown in Figure 4 where the second and third π^* resonances are visible (the first π^* resonance is of $^2A_2$ symmetry). For the avoidance of confusion, from now on we will refer to the "4.7 eV" resonance when referring to the third π^* resonance (i.e. the second one visible in Fig. 4). The contributions in Figure 4 are determined omitting selected T-matrix elements from the expression (2) for the integral cross section.

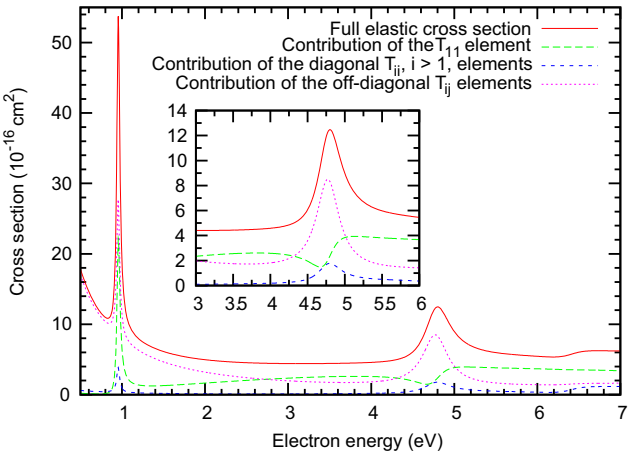

Fig. 4. Contributions of the $^2B_1$ T-matrix elements to the integral elastic cross section. Full red line: full $^2B_1$ contribution to the integral elastic cross section; dashed green line: contribution of the T_{11} element; dotted blue line: contribution of the diagonal T_{ii}, $i > 1$ elements; dotted pink line: contribution of the off-diagonal T_{ij} elements. The inset shows the detail of the energy range between 3 to 6 eV where the 4.7 eV resonance appears.

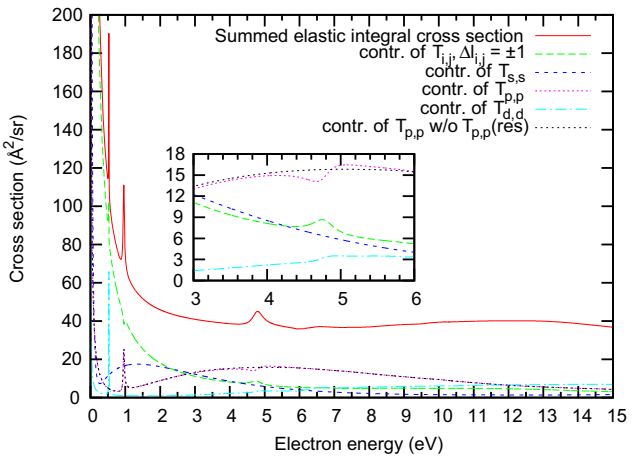

Fig. 5. Contributions of selected types of T-matrix elements to the summed integral cross section. Red line: summed integral cross section including all T-matrix elements. Green dashed line: contribution of T-matrix elements T_{ij} with $\Delta l_{ij} = \pm 1$. Dashed blue line: contribution of the T-matrix element $T_{s,s}$ (i.e. $T_{l=0,m=0;l'=0,m'=0}$). Dotted magenta line: contribution of the $T_{p,p}$ elements. Dotted-dashed light blue line: contribution of the $T_{d,d}$ elements. Dotted black line: contribution of the $T_{p,p}$ elements with the resonant contribution around the 3rd π^* resonance removed. The inset shows in detail the energy region corresponding to the 4.7 eV resonance.

The first π^* resonance in this symmetry has the same qualitative behaviour (a peak) in all the contributions. However, not all T-matrix elements have the same qualitative behaviour in the vicinity of the 4.7 eV resonance: unlike the others, the T_{11} amplitude (one component of the p-wave to p-wave scattering) does not contribute as a peak but as a dip/peak structure. No doubt this is due to an interference between the background and the resonant parts comprising the T_{11} matrix element. In the full $^2B_1$ contribution (red line in Fig. 4), the shoulder caused by the T_{11} element leads to the resonant peak being non-symmetrical and its maximum being shifted slightly towards higher energy with respect to the peak caused by the rest of the T-matrix elements (incidentally, one can also observe that it is the off-diagonal elements that are mainly responsible for the strong rise of the cross section at lower energies as expected: the dipolar interaction couples partial waves with $\Delta l = \pm 1$).

The calculation of the DCS requires combining T-matrix elements for all scattering symmetries. This gives rise to the possibility of a significant interference between partial waves coming from different scattering symmetries. To estimate the importance of the T-matrix elements from the other symmetries, we calculated the summed integral cross sections taking into account only the dominant subsets of all T-matrix elements. These are shown in Figure 5.

We can see that the contribution from the mostly dipole-induced transitions between partial waves differing by one unit of angular momentum (green dashed line) is the one that most influences the shape of the cross section at low electron energies below approx. 3 eV. At higher energies, the other important contribution comes from the background p-wave to p-wave scattering ($^2A_1$, $^2B_1$ and $^2B_2$ scattering symmetries; note that when all 3 symmetries are included the $T_{p,p}$ contribution is much bigger than when only the $^2B_1$ p-wave to p-wave T-matrix element is taken into account) and from the s-wave to s-wave scattering ($^2A_1$ symmetry). In particular, the p-wave background scattering (dotted black line) attains a maximum almost exactly at the location of the 3rd π^* resonance. We have already established that the contribution of the p-wave to p-wave scattering amplitude to the integral cross section in the $^2B_1$ symmetry is significantly affected by the interference between its background and resonant parts, see green dashed line in Figure 4. The existence of this interference together with the large magnitude of the components of the p-wave to p-wave scattering amplitudes from the other symmetries leads to the hypothesis that the asymmetry in the angular distributions for this resonance is caused by interference between the background p-wave to p-wave and the resonant scattering amplitudes for the 3rd π^* resonance.

In order to test this hypothesis, we performed fits of the $^2B_1$ T-matrix elements in the energy range 3 to 6 eV to the resonant formulae [21]:

$$T_{ij}(E) = T_{ij}^{bg}(E) + T_{ij}^{res}(E), \tag{4}$$

$$T_{ij}^{res}(E) = -\frac{a_{ij}^2}{E - E_R + \imath\Gamma/2}, \tag{5}$$

$$T_{ij}^{bg}(E) = A_{ij} + B_{ij}E, \tag{6}$$

where A_{ij}, B_{ij}, E_R, Γ and a_{ij} are the fitting parameters (E_R and Γ being the resonance position and width). Formally, the parameters a_{ij} are determined using the partial widths, γ_i, for entering/leaving the resonance [21]:

$$a_{ij} = \gamma_i\gamma_j. \tag{7}$$

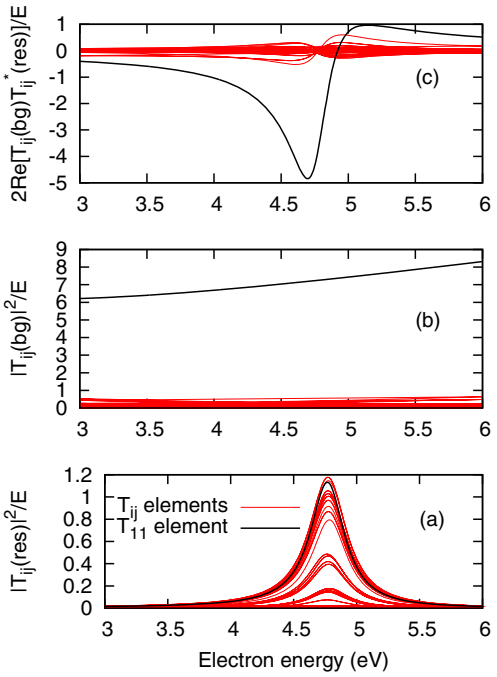

Fig. 6. Contributions to the integral cross section for $^2B_1$ symmetry in the energy region of the 4.7 eV resonance: (a) resonant, $|T_{ij}^{res}|^2/E$, (b) background, $|T_{ij}^{bg}|^2/E$ and (c) cross resonant/background, $2\mathrm{Re}[T_{ij}^{bg}T_{ij}^{res*}]/E$. The contributions of the T-matrix element T_{11} are plotted using a black line and those of T_{ij}, $\{i,j\} \neq \{1,1\}$ using a red line.

For simplicity we have treated the a_{ij} independently of each other. We are justified in doing so since we are not interested in the partial widths but only in separating the resonant, T_{ij}^{res}, and the background, T_{ij}^{bg}, contributions to the T-matrix elements.

The obtained resonant, background and cross terms (i.e. $2\mathrm{Re}[T^{bg}T^{res*}]/E$) are shown in Figure 6. We can clearly identify a strong background contribution to the scattering amplitude T_{11} which describes p-wave to p-wave scattering. In comparison, the background contributions in all other channels are an order of magnitude smaller (see Fig. 6b), and do not cause a significant dip/peak behaviour of the resonant/background cross terms in the vicinity of the resonance, see Figure 6c.

These results explicitly demonstrate that the slight asymmetry of the resonant peak in the integral cross section in the vicinity of the resonance is due to coherent superposition of the background and resonant scattering amplitudes in the p-wave to p-wave channel in the $^2B_1$ symmetry.

To analyze the DCS in the vicinity of the resonance we separate the T-matrix elements into their resonant and background parts (see Eq. (4)), and investigate the effect various interferences between the background and the resonant scattering amplitudes have on the dip/peak (or peak/dip) shape of the angular distributions.

We begin by removing from calculation of the DCS those terms corresponding to the interference of the background, $T_{p,p}^{bg}(^2B_1)$, and resonant, $T_{p,p}^{res}(^2B_1)$, parts of the T_{11} element in the $^2B_1$ symmetry. The resulting excitation functions are shown in Figure 7 (red line). We can see that while contribution of these terms to the backward scattering is non-negligible their absence does not lead to the removal of the asymmetry in the excitation functions for the forward and backward direction (although their removal has the expected effect of removing the dip/peak structure from the integral cross section as Fig. 4 implies). The asymmetry is somewhat reduced by removing all interference terms of the type $T_{p,p}^{bg}(^2B_1)T_{all,all}^{res*}(^2B_1) + c.c.$ (dashed green line) suggesting that the background p-wave to p-wave scattering amplitude from the $^2B_1$ symmetry interferes with a number of resonant amplitudes (not only with $T_{p,p}^{res}$).

In the final step we remove all interference terms of the type $T_{p,p}^{bg}T_{all,all}^{res*} + c.c.$ (see Fig. 7). Note that this requires removing interferences originating in the T-matrix elements of the $^2A_1$ and $^2B_2$ symmetries which contain the rest of the p-wave scattering channels $\{l,m\} = \{1,0\}$ and $\{1,-1\}$ respectively. We observe that removing these interference terms removes almost perfectly the asymmetry in the excitation functions for the forward and backward directions.

The angular distributions for the forward/backward direction obtained using this procedure are shown in Figure 8. Indeed we observe a symmetric resonant peak superimposed on a smooth background, as is particularly obvious if this figure is compared to Figure 3. We conclude that the dip/peak and peak/dip structure in the angular distributions is caused predominantly by an interference of the strong background p-wave to p-wave scattering amplitude with the amplitudes for resonant scattering. We note that the resonant peak becomes slightly more symmetric when removing, in addition to those mentioned above, interferences between the resonant and the background s-wave to s-wave scattering (not shown).

Interestingly, while forming at lower electron energies, the second π^* resonance (i.e. the first resonance of $^2B_1$ symmetry, appearing at $\simeq$1 eV) shows only a very small modulation of its shape in the integral cross sections due to the superposition of the background and resonant scattering amplitudes. A small dip/peak modulation in the DCS appears only in the forward direction. This resonance is significantly narrower and appears predominantly in the T_{11} matrix element which is also the one responsible for the small asymmetry of the resonant peak in the integral cross sections. However, it can be inferred from Figures 4 and 5 that in the resonant energy region the background p-wave to p-wave contribution passes through a minimum and therefore its superposition with the resonant amplitude is minimized.

To further confirm our understanding of the interference effects we have performed, for this first resonance in the $^2B_1$ symmetry, the same background/resonant partitioning of the T-matrix elements and found that removing the interferences between the background p-wave to p-wave amplitudes and the resonant scattering amplitudes eliminates the small asymmetry in the DCS in the forward direction but introduces a slight asymmetry in the

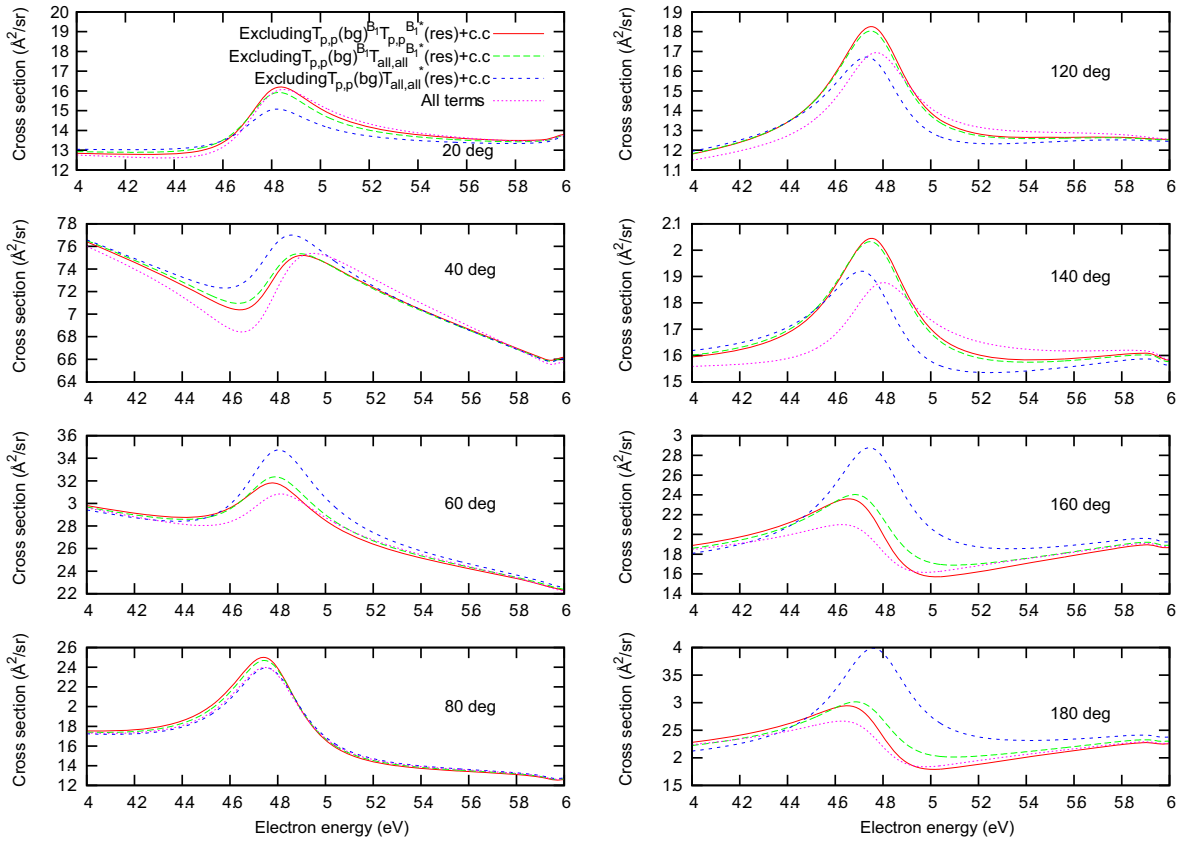

Fig. 7. Excitation functions calculated removing various interference terms. Dotted pink line: all terms included; red full line: the term $T_{p,p}^{bg}T_{p,p}^{res*} + c.c.$ of $^2B_1$ symmetry is excluded; dashed green line: the terms $T_{p,p}^{bg}T_{all,all}^{res*} + c.c.$ of $^2B_1$ symmetry is excluded; blue dashed line: the terms $T_{p,p}^{bg}T_{p,p}^{res*} + c.c.$ for all symmetries is excluded. Here "*c.c*" denotes the complex conjugate.

backward direction. Removing, in addition to the previous terms, interferences between the background s-wave to s-wave and resonant amplitudes restores the symmetry of the resonant peak in the backward direction while keeping the symmetry of the forward peak unaffected. This suggests that, for the ≃1 eV resonance, there are two small but competing interference effects at play: interference between the background s-wave to s-wave and resonant scattering amplitudes and interference between the background p-wave to p-wave and resonant scattering amplitudes. The contribution of the s-wave background scattering to the interference with the resonant amplitude is not surprising since the s-wave background peaks close to the energy of the resonance (see Fig. 5). However, whether a given background scattering amplitude will play a significant role in the interference with the resonant one depends not only on the magnitude of its contribution to the cross section but crucially on its phase with respect to the resonant amplitude.

5 Conclusions

We have analyzed the structure present in the excitation functions of electron scattering from pyrimidine in the energy range corresponding to the third π^* resonance.

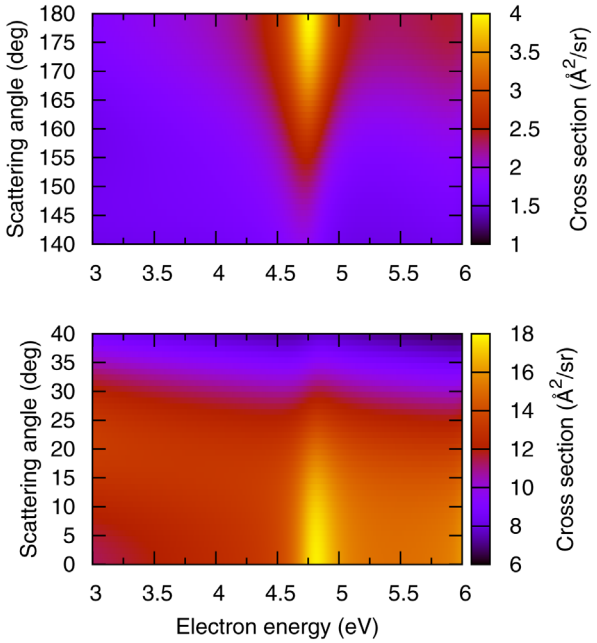

Fig. 8. Detail of the angular distributions in the energy range of the 4.7 eV resonance for forward (lower panel) and backward (upper panel) scattering with the interference terms $T_{p,p}^{bg}T_{all,all}^{res*} + c.c.$ removed. Note that the colour scales are different for each panel.

We conclude that the structure is due to the coherent superposition of the background p-wave to p-wave elastic scattering amplitudes and the elastic resonant scattering amplitudes (for all partial waves) in that energy range. The structure is not linked to the mixed core-excited shape character of the resonance and could therefore be present in other resonances both in this and other systems. Indeed, we have also analyzed the data for electron collisions with the non-polar molecule pyrazine obtained in our previous work [22] and found the same asymmetry in angular distributions in the vicinity of the third π^* resonance. We have also shown that the background contribution responsible for the asymmetry of the third π^* resonance (around 4.7 eV) is weak in the energy region of the first resonance of the same symmetry (around 1 eV) explaining why, for this first resonance, the variation of the shape of the excitation functions with the scattering angle is negligible.

We note that this effect can affect the comparison of theory and experiment: the background contribution to the scattering depends relatively strongly on energy so that shifting the resonance position away from where it is observed in the experiment will result in a significant modification of the relative phase between the background and the resonant phase shifts. Consequently the dip/peak structure in the angular distributions will be modified. Therefore, it is obvious from this analysis that the agreement with experiment will depend on the ability of the calculation to reproduce the resonance position fairly well. The difference of around 0.3 eV between our calculations and experiment seems good enough in this case.

We are extremely grateful to Prof. Michael Allan who encouraged us to look at our calculations in more detail and, in doing so, seek a deeper understanding of the physics being described. Additionally, Z.M. acknowledges useful discussions with Dr Alex Harvey. This work was supported by EPSRC and the ARCHER eCSE01-013 project; Z.M. acknowledges the use of the VULCAN computer cluster at the Max-Born Institute.

References

1. P. Palihawadana, J. Sullivan, M. Brunger, C. Winstead, V. McKoy, G. García, F. Blanco, S. Buckman, Phys. Rev. A **84**, 062702 (2011)
2. A. Modelli, P. Bolognesi, L. Avaldi, J. Phys. Chem. A **115**, 10775 (2011)
3. D.B. Jones, S.M. Bellm, F. Blanco, M. Fuss, G. Garcia, P. Limão-Vieira, M.J. Brunger, J. Chem. Phys. **137**, 074304 (2012)
4. D.B. Jones, S.M. Bellm, P. Limão-Vieira, M.J. Brunger, Chem. Phys. Lett. **535**, 30 (2012)
5. M. Neustetter, J. Aysina, F.F. da'Silva, S. Denifl, Angew. Chem. Int. Ed. **54**, 9124 (2015)
6. A.S. Barbosa, D.F. Pastega, M.H.F. Bettega, J. Chem. Phys. **143**, 244316 (2015)
7. C. Winstead, V. McKoy, Phys. Rev. A **76**, 012712 (2007)
8. Z. Mašín, J.D. Gorfinkiel, D.B. Jones, S.M. Bellm, M.J. Brunger, J. Chem. Phys. **136**, 144310 (2012)
9. Z. Mašín, J.D. Gorfinkiel, J. Chem. Phys. **137**, 204312 (2012)
10. A. Sanz, M. Fuss, F. Blanco, Z. Mašín, J.D. Gorfinkiel, F. Carelli, F. Sebastianelli, F. Gianturco, G. García, Appl. Rad. Isotopes **83**, 57 (2014)
11. B. Boudaïffa, P. Cloutier, D. Hunting, M.A. Huels, L. Sanche, Science **287**, 1658 (2000)
12. I. Baccarelli, I. Bald, F.A. Gianturco, E. Illenberger, J. Kopyra, Phys. Rep. **508**, 1 (2011)
13. I. Nenner, G.J. Schulz, J. Chem. Phys. **62**, 1747 (1975)
14. K. Regeta, M. Allan, C. Winstead, V. McKoy, Z. Mašín, J.D. Gorfinkiel, J. Chem. Phys. **144**, 024301 (2016)
15. K. Regeta, M. Allan, Z. Mašín, J.D. Gorfinkiel, J. Chem. Phys. **144**, 024302 (2016)
16. J. Tennyson, Phys. Rep. **491**, 29 (2010)
17. P.G. Burke, *R-Matrix Theory of Atomic Collisions: Application to Atomic, Molecular and Optical Processes* (Springer, 2011)
18. J.M. Carr, P.G. Galiatsatos, J.D. Gorfinkiel, A.G. Harvey, M.A. Lysaght, D. Madden, Z. Mašín, M. Plummer, J. Tennyson, H.N. Varambhia, Eur. Phys. J. D **66**, 58 (2012)
19. N. Sanna, F.A. Gianturco, Comput. Phys. Commun. **114**, 142 (1998)
20. H.J. Werner et al., MOLPRO, version 2009.1, a package of ab initio programs (2009)
21. J.R. Taylor, *Scattering theory: The quantum theory on nonrelativistic collisions* (Dover, 2006)
22. Z. Mašín, J.D. Gorfinkiel, J. Chem. Phys. **135**, 144308 (2011)